

Low Coherence Vibration Insensitive Fizeau Interferometer

Brad Kimbrough, James Millerd, James Wyant, John Hayes

*4D Technology Corporation, 3280 E. Hemisphere Loop, Suite 146, Tucson, AZ 85706
(520) 294-5600, (520) 294-5601 Fax, brad.kimbrough@4dtechnology.com*

An on-axis, vibration insensitive, polarization Fizeau interferometer is realized through the use of a novel pixelated mask spatial carrier phase shifting technique in conjunction with a low coherence source and a polarization delay-line. In this arrangement, coherence is used to effectively separate out the orthogonally polarized test and reference beam components for interference. With both the test and the reference beams on-axis, the common path cancellation advantages of the Fizeau interferometer are maintained. The interferometer has the unique ability to isolate and measure any surface that is substantially normal to the optical axis of the cavity. Additionally, stray light interference is substantially reduced due to the source's short coherence. An expression for the fringe visibility on-axis is derived and compared with that of a standard Fizeau. Using a 15 mW source, the maximum camera shutter speed, used when measuring a 4% reflector, was 150 usec, resulting in very robust vibration insensitivity. We experimentally demonstrate the measurement of both sides of a thin glass plate without the need to modify the plate between measurements. Experimental results show the performance of this new interferometer to be within the specifications of commercial phase shifting interferometers.

Introduction

Determination of the spatial variations of optical phase is of primary importance in the fields of optical testing and metrology, optical information processing, and adaptive optics. There exist several techniques for the encoding of spatial phase modulation in fringe patterns and the subsequent analysis of these fringe patterns for a quantitative determination of phase.¹ The two primary groups of fringe pattern analysis techniques are: Temporal phase measurement, sometimes known as the phase shifting method, and spatial phase measurement which is also called the spatial carrier method.

Temporal phase measurement is a well-established method for measuring optical wavefront phase². In this technique, three or more interferogram intensity profiles are recorded. For each recording, there is a different relative phase between the test and reference beams. The phase distribution of the test wavefront is then calculated using the recorded interferogram intensities. DeGroot, et. al demonstrated the measurement of multiple surfaces within a cavity using wavelength tuning and temporal phase-shifting³.

Spatial phase measurement utilizes a single interferogram to extract phase information.⁴ In this technique, a spatial carrier, typically in the form of high frequency tilt fringes, is applied to the interferogram. The intensity profile of the modulated spatial carrier interferogram is recorded and then analyzed to determine the phase. The primary advantage of the spatial phase measurement technique over temporal phase measurement is that only one image is required, allowing acquisition times several orders of magnitude smaller than in temporal phase shifting. Rapid acquisition offers both significant vibration immunity, and the ability to measure dynamic events.

A novel approach to spatial phase measurement has been developed by 4D Technology Corporation called the *pixelated mask spatial carrier method*.⁵ In this technique, the relative phase between carrier and test wavefront is modified on a pixel-by-pixel basis by a micro-polarizer phase shifting array placed just prior to detection. This technique requires that the test and reference beams be orthogonally polarized. This is easily implemented in a Twyman-Green interferometer that uses a polarizing beam splitter to separate the source wavefront into orthogonally polarized test and reference beams. In the Fizeau interferometer, the test and reference beams are not separated as in the Twyman-Green, but travel along a common-path up to the reference surface. Due to this almost common path arrangement, the configuration of the Fizeau interferometer is substantially simpler and only the reference surface must be produced with a high optical precision. The main drawback with this arrangement is that the overlapping test and reference beams make it difficult to implement a polarization Fizeau interferometer.

One solution to this problem has been implemented by 4D Technologies and is called the tilted beam Fizeau.⁶ In this arrangement, a relatively large tilt angle is placed on the reference flat giving a large angular offset between the test and reference beams. Prior to incidence on the pixelated mask sensor, the two beams pass through a Wollaston prism, producing two pairs of orthogonally polarized test and reference beams. Only one of these beam pairs is collinear with each other and with the optical axis. The major drawback with this technique is that with the tilted reference surface, the returning test and reference beams no longer follow a common path, resulting in retrace errors in the measurement. For plano reference and test optics the interferometer can be designed to have very low retrace errors; however, the use of transmission spheres can introduce substantial errors and calibration techniques must be used.

Kuchel proposed the use of a low temporal coherence source and an optical delay-line that splits the source beam into two orthogonally polarized components and allows a controllable phase difference between the two beams.⁷ In this paper we report on combining the delay-line Fizeau configuration with 4DTechnology's pixelated-mask instantaneous phase sensor. The benefits of the resulting instrument are three fold. First, the systems permits high spatial resolution instantaneous phase measurement in a single camera frame. Secondly, the two orthogonally polarized beams are collinear – allowing true on-axis operation so that transmission flats and spheres can be used without calibration. Finally, the delay line allows matching of the reference and test beam optical paths, facilitating the measurement of specific surfaces within an optical cavity. For

example, the measurement of transparent surfaces such as thin lenses or plates can be made by suppressing the interference due to reflection from the back surface.^{8, 9} Additionally, the use of very low temporal coherence sources reduces coherent system noise due to spurious reflections. We present the theory of operation of the instrument and results obtained measuring both sides of an uncoated glass plate using only two measurements and without the need to modify the plate.

Theory of Operation

The basic layout of the short coherence vibration insensitive Fizeau is shown in figure 1. The illumination system is composed of a short coherence laser source and an optical delaying device that splits the source beam into two orthogonally polarized components and applies a controllable optical path difference between the two beams. This output is used as the illumination source for a standard Fizeau interferometer arrangement. The output of the Fizeau is imaged via an afocal imaging system onto the pixelated mask sensor.

The optical delaying device is essentially a polarization Twyman-Green interferometer. It is convenient to think of the illumination as being composed of two separate but overlapping beams, the *s*-polarized beam and the *p*-polarized beam. The half wave plate just in front of the laser source is used to adjust the intensity ratio between the two beams. As will be shown in the next section, maximum visibility is obtained when the intensities of the *s* and *p* components are matched, regardless of the test and reference mirror reflectivities. Upon exiting the optical delaying device, there is an optical path delay between the *s*-polarized and the *p*-polarized beams. Mirror M1 is mounted to a stage and allows the optical path length of the exiting *p*-polarized beam to be adjusted relative to that of the *s*-polarized beam which originates from M2.

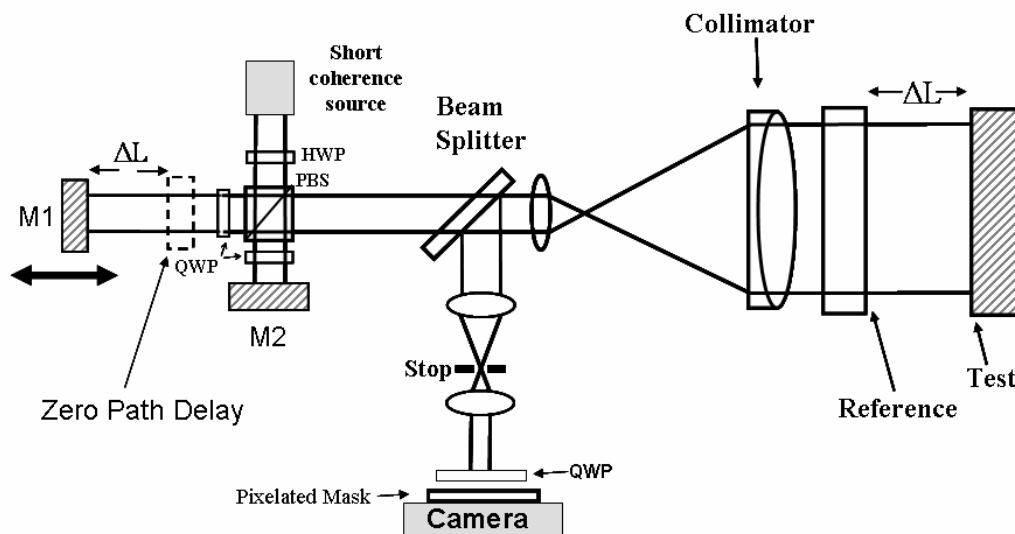


Figure 1: Short coherence vibration insensitive Fizeau functional diagram.

Both the s and p -polarized beams illuminate and are reflected by the test and reference surfaces. The returning beams undergo reflection at the non polarizing beam splitter and are imaged via an afocal imaging system onto the pixelated mask sensor. The quarter wave plate, QWP, just prior to the pixelated mask is used to convert the linearly polarized test and reference beams into right and left circular polarizations as is necessary for the operation of the pixelated mask sensor.

Ignoring multiple Fizeau cavity reflections for the moment, there are essentially 4 beams incident upon the pixelated mask sensor; s and p -polarized test surface reflected beams, and s and p -polarized reference surface reflected beams. For the pixelated mask sensor we would like interference to occur between either the s -polarized reference beam and the p -polarized test beam, or between the p -polarized reference beam and the s -polarized test beam. Since the source has a very short coherence length, approximately 250 μm , only those beams whose optical paths, from the source to the camera, have been matched will interfere. No interference will occur between the other beam pair and there intensities will simply add to the background.

Visibility

Figure 2 shows a Fizeau cavity with flat and parallel test and reference surfaces whose reflectivities are R_t and R_r respectively. The cavity is illuminated with both s (I_s - top) and p (I_p - bottom) polarized light. Both beams are collinear, but have been separated for clarification. The s -polarized beam is delayed such that its reflection off of the reference surface is path matched to the p -polarized beams first reflection off of the test surface. Both of these beams are shown as solid red lines pointing to the right.

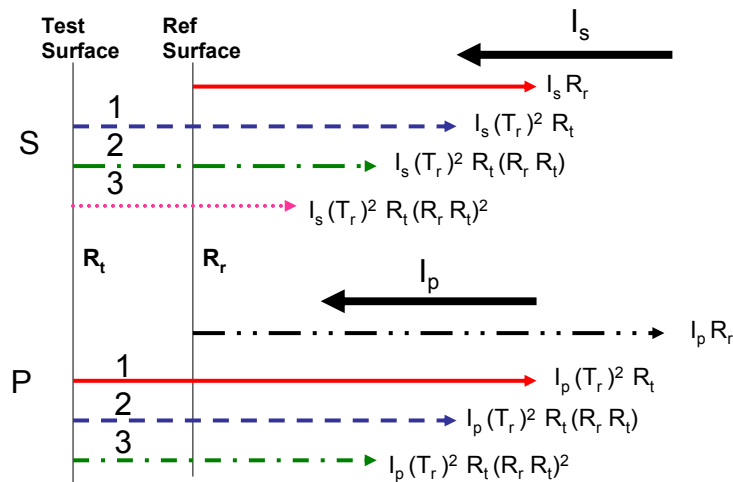


Figure 2: Multiple test surface reflections in the low coherence Fizeau cavity

The bold numbers within the cavity indicates the number of test surface reflections each beam has undergone prior to exiting the cavity. Path matched, coherent, beams are of similar color and type, (e.g. red-solid, blue-dashed). The formula to the right of the beams indicates their intensities. Note that there are more than one set of interfering beams and that each beam is coherent with only one other beam. Each coherent pair will interfere, producing a fringe pattern. The primary interference pattern is created by the interference of the *s*-polarized beam from the reference surface and the *p*-polarized beam that has reflected once from the test surface, solid red lines. The next coherent beam pair is composed of the *s*-polarized beam that has reflected once from the test surface, and the *p*-polarized beam that has reflected twice from the test surface, blue dashed lines. Each successive reflection of the *s*-polarized beam off of the test surface is coherent with the *p*-polarized beam that has undergone one additional test surface reflection. The interferogram detected at the output of the interferometer is composed of the sum of the primary fringe pattern with the fringe patterns of the other coherent beam pairs. This fringe pattern can be represented mathematically as:

$$\begin{aligned}
 I = & I_{pr} + I_{sr} + I_{pt[1]} + 2\sqrt{I_{pt[1]}I_{sr}} \text{Cos}[\theta_1] \\
 & + I_{st[1]} + I_{pt[2]} + 2\sqrt{I_{st[1]}I_{pt[2]}} \text{Cos}[\theta_2] + \dots \\
 & + I_{st[n-1]} + I_{pt[n]} + 2\sqrt{I_{st[n-1]}I_{pt[n]}} \text{Cos}[\theta_n] + I_{st[n]}
 \end{aligned} \tag{1}$$

where I_{pr} and I_{sr} are the intensities of the *p* and *s*- polarized beams reflected off of the reference surface, $I_{pt[n]}$ and $I_{st[n]}$ are the intensities of the *p* and *s*-polarized beams that have undergone *n* reflections off of the test surface, and θ_n is the phase difference between the *n*th pair of interfering beams.

Writing equation 1 in terms of the reference and test surface reflectivity, R_r and R_t , and separating the constant terms from the interference terms gives:

$$\begin{aligned}
 I = & (I_s + I_p) (R_r + (1-R_r)^2 R_t [1 + (R_r R_t) + \dots + (R_r R_t)^{n-1}]) \\
 & + 2 (1-R_r) \sqrt{R_t R_r} \sqrt{I_s I_p} \text{Cos}[\theta_1] \\
 & \underline{n \geq 2} \\
 & + 2 (1-R_r)^2 R_t \sqrt{R_t R_r} \sqrt{I_s I_p} (\text{Cos}[\theta_2] + (R_t R_r) \text{Cos}[\theta_3] + \dots + (R_t R_r)^{n-2} \text{Cos}[\theta_n])
 \end{aligned} \tag{2}$$

Simplifying the geometric series in the first term of equation 2 gives:

$$I = (I_s + I_p) \left(R_r + T_r^2 R_t \frac{1 - (R_r R_t)^n}{1 - (R_r R_t)} \right) + 2 (1 - R_r) \sqrt{I_s I_p} \sqrt{R_t R_r} \cos[\theta_1] \quad (3)$$

$$\underline{n \geq 2}$$

$$+ 2 (1 - R_r)^2 R_t \sqrt{I_s I_p} \sqrt{R_t R_r} \left(\cos[\theta_2] + (R_t R_r) \cos[\theta_3] + \dots + (R_t R_r)^{n-2} \cos[\theta_n] \right)$$

In order to evaluate equation 3 further, the phases of the interference terms must be determined. These phase terms are a function of the test surface shape, and the separation of the test and reference surfaces. In the simplest case, the cavity is nulled and the test and reference surfaces are close to parallel at every point. In this case it can be shown that the phase difference between all secondary interfering beam pairs, θ_n , is equal to $-\theta_1$. The negative sign resulting from the fact that for the secondary interfering beam pairs, all reflections occur at an air to glass interface, whereas for the primary interfering beam pair, the reference beam results from a glass to air interface reflection off of the reference surface. Setting $\theta_n = -\theta_1$, and taking the limit as n becomes very large, equation 3 reduces to:

$$I = (I_s + I_p) \left(R_r + \frac{(1 - R_r)^2 R_t}{1 - R_r R_t} \right) + 2 (1 - R_r) \sqrt{I_s I_p} \sqrt{R_t R_r} \left(\frac{(1 - R_t)}{1 - R_t R_r} \right) \cos[\theta_1] \quad (4)$$

From equation 4, the fringe visibility is determined to be:

$$Vis = \left(\frac{\sqrt{I_s I_p}}{I_s + I_p} \right) \frac{(1 - R_r)(1 - R_t) \sqrt{R_t R_r}}{(1 - R_r) R_t + (1 - R_t) R_r} \quad (5)$$

A plot of fringe visibility as a function of test surface reflectivity for three different values of reference surface reflectivity is shown in figure 3. Visibility curves for a standard Fizeau arrangement are also shown for comparison.

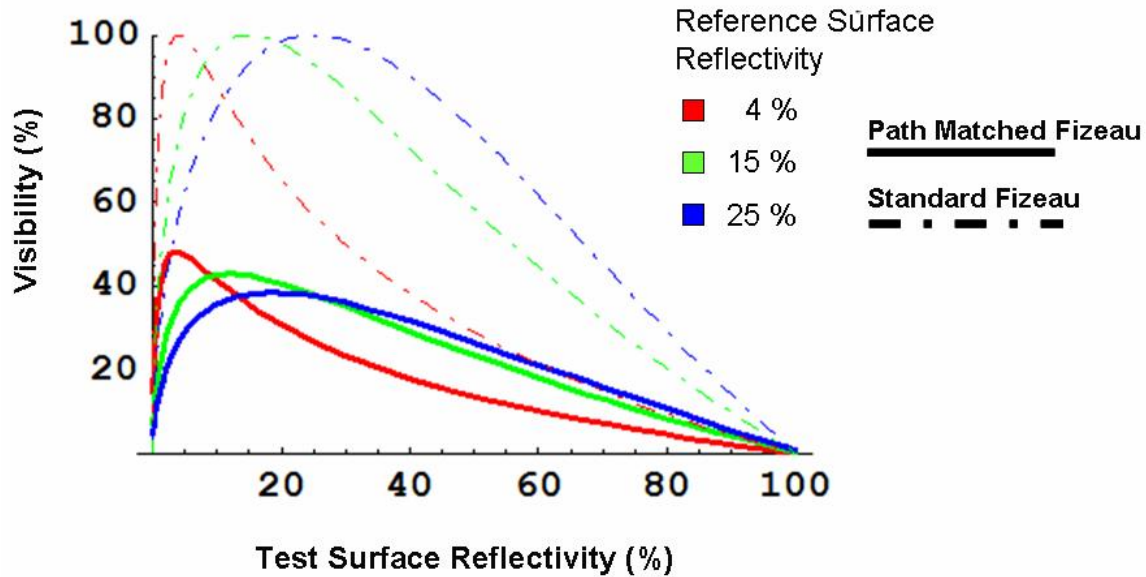


Figure 3: Visibility versus test surface reflectivity for the low coherence Fizeau.

For these plots $I_s = I_p$. Unlike a standard polarization interferometer, matching the test and reference beam intensities at the interferometer output will not maximize fringe contrast. Beam balance affects the first term in equation 5, and this term maximized when the illumination beam intensity ratio is equal to one. Fringe visibility is maximized when test and reference surface reflectivities are nearly matched. As can be seen from the plot, the maximum fringe visibility is obtained at low reference surface reflectivities. As the reference surface reflectivity is increased, the maximum fringe visibility is reduced. Additionally, like the standard Fizeau, multiple cavity reflections results in a loss of fringe contrast for high test surface reflectivities.

Optical Configuration

A diagram of the low coherence Fizeau prototype that was built is shown in figure 4. The prototype is composed of three major sections: (1) A custom designed low coherence source, including spatial filtering and collimation, (2) polarization path matching, and (3) Fizeau cavity and imaging system. The source filtering and collimation section consists of the laser diode, a spatial filter, and a collimating lens. The laser diode output is 15 mW at 658 nm. The coherence length of this source is approximately 250 μm FWHM.

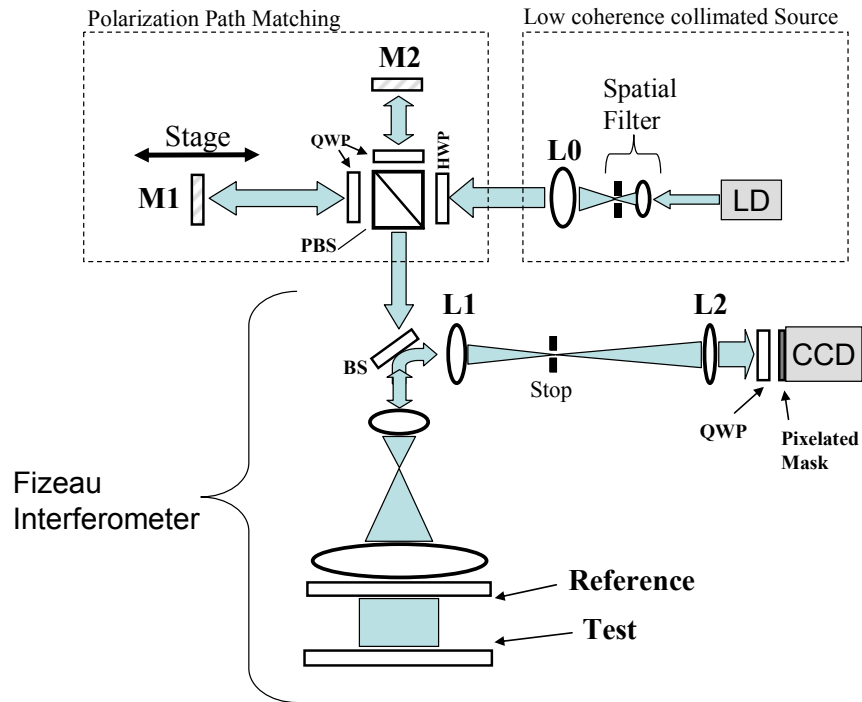


Figure 4: Low coherence Fizeau prototype.

The polarization path matching section is essentially a polarization Twyman-Green interferometer and consists of a half wave plate, HWP, a polarizing beam splitter, PBS, two quarter wave plates, QWP, a fixed mirror, M2, and a mirror mounted to a linear stage, M1. The two proceeding components constitute the source for the interferometer. The output of the path matching section is a collimated beam with a diameter of approximately 14 mm. This beam first passes through a non-polarizing beam splitter, BS, and then a diverging lens and a collimation lens, producing a collimated beam with a diameter of approximately 100 mm. This beam is then reflected off of the reference and test surfaces and returns to the beam splitter. A portion of this beam is then reflected towards the afocal imaging system composed of L1, L2, and an aperture stop. L1 and L2 have focal lengths of 100 and 200 mm respectively, giving a magnification of 2. Prior to the pixelated mask and CCD, the input beam passes through a QWP changing the linear s -polarized and p -polarized components into right and left circular polarizations.

Transparent Glass Disk Measurements

To demonstrate the utility of the interferometer we made measurements on thin glass plates, a test that is virtually impossible with conventional Fizeau interferometers because of multiple reflections. Figure 5 shows three possible measurements that can be made on a transparent glass plate without turning the test piece around. Designate one side of the plate as side A, and the other as side B. The diagram on the left side of the figure shows

the transparent glass plate with a side A height profile, h_a , a nominal thickness of t_o , and a side B surface height profile of h_b . For measurement (1), side A is facing the reference surface and has been path matched. The measured height profile, H , is equal to the defect height profile, h_a . In measurement (2), side A is facing the reference surface, but now side B has been path matched. The measured height, H , is now given by:

$H = h_a - n(h_a + h_b)$, where n is the glass index of refraction and is assumed to be constant.

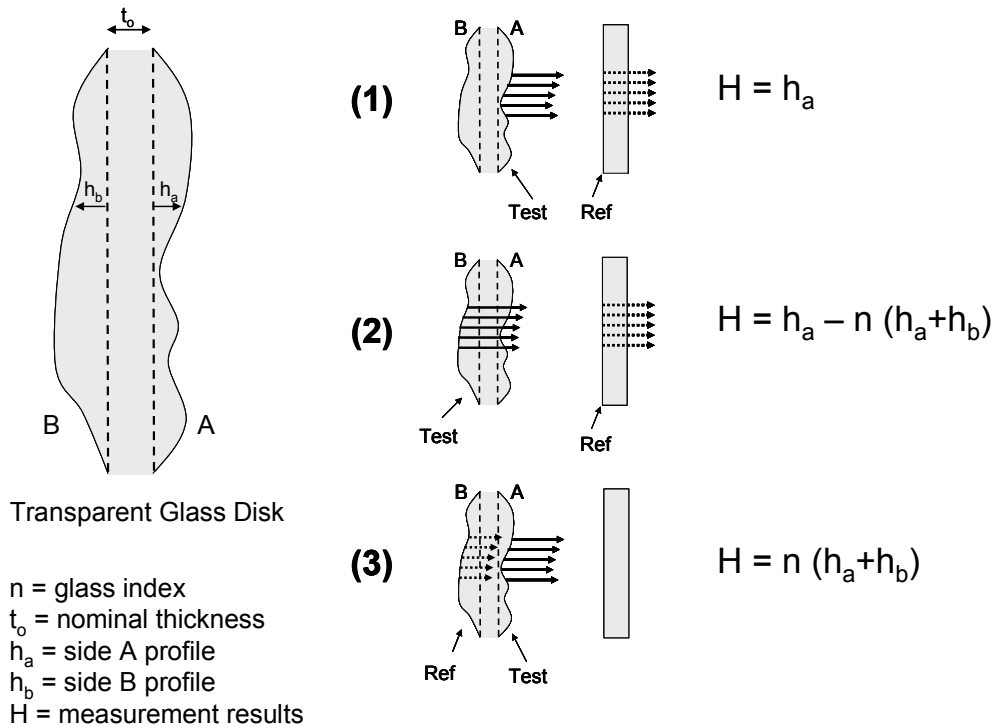


Figure 5: Transparent Glass Plate Test Arrangements. In test (1) side A is path matched with the reference surface. In test (2) side B is path matched with the reference surface. In test (3) side A is path matched with side B.

For measurement (3), side A has been path matched to side B and the surface measurement result is given by: $H = n(h_a + h_b)$, where once again the glass index is assumed constant. The transmission flat (external reference surface) can be removed for this measurement.

Experimental Results

Measurements (1)-(3) as outlined above were conducted on a four inch diameter glass disk having a nominal thickness, t_o , of 1 mm. All measurements were carried out on a rigid optical table and no steps were taken to control environmental vibrations. Figure 6 provides the results of measurements (1) and (2) on the left and right sides respectively. Note that measurement (2) does not directly provide the surface height profile of side B.

Letting H_1 and H_2 be equal to the results of measurements (1) and (2) respectively, the surface height profile of side B, h_b can be calculated as follows:

$$h_b = \frac{1}{n}(H_1 - H_2) - H_1 \quad (6)$$

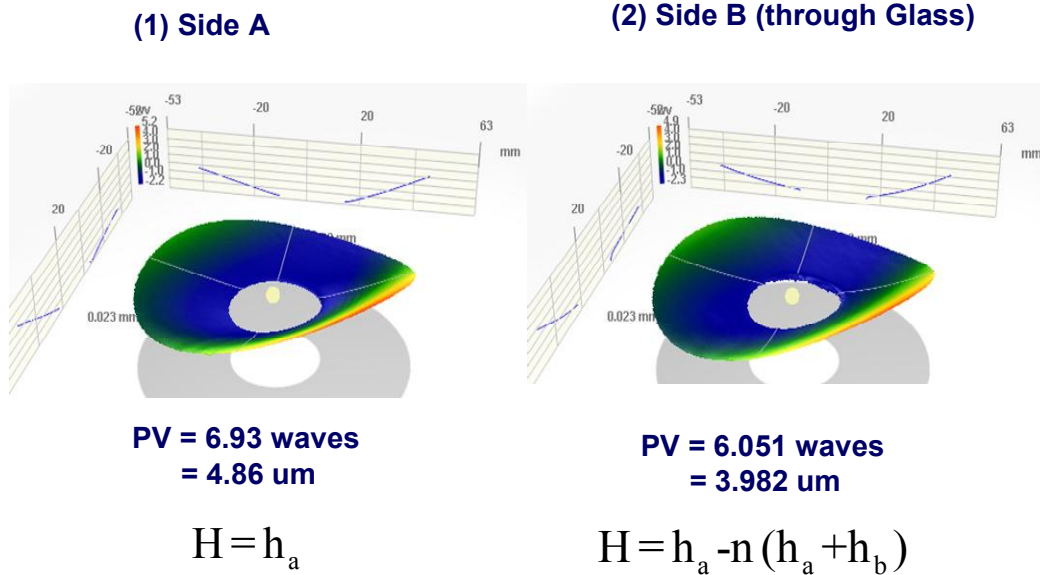


Figure 6: Transparent glass disk measurement results for test arrangements (1) and (2).

Using an index of refraction equal to 1.5, the surface height profile of side B was calculated from the results of measurements (1) and (2). Figure 7 shows this result along with a direct measurement of the side B profile obtained by turning the test piece around and path matching side B to the reference surface. Both the direct and calculated measurements are in close agreement, indicating that both surface profiles, h_a and h_b , can be determined without turning the disk around.

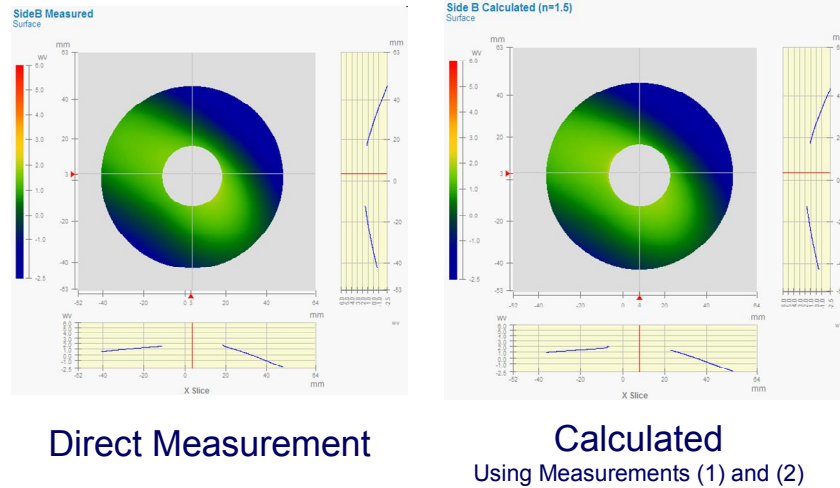


Figure 7: Comparison of a direct measurement of the side B surface profile with the surface profile calculated from the results of measurements (1) and (2).

Figure 8 shows the results of measurement (3). This measurement was conducted by path matching side A to side B. This measurement can be interpreted as the optical thickness deviation about the nominal disk thickness. Since the reference flat is not used in this measurement, it may be removed from the system. Because beams reflected off of the reference flat add to the non-coherent background intensity, its removal will result in an increase in the fringe contrast.

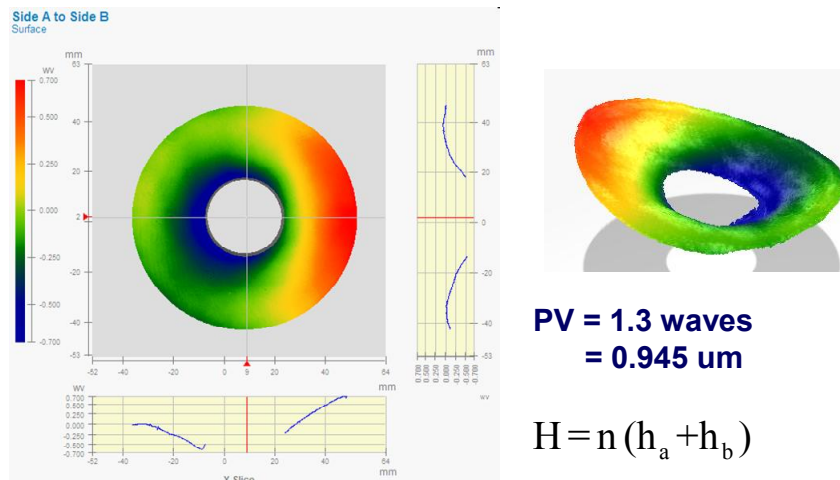


Figure 8: Transparent glass disk measurement results for test arrangement (3).

Conclusions

An on-axis, vibration insensitive, polarization Fizeau interferometer has been realized through the use of a novel pixelated mask spatial carrier phase shifting technique in

conjunction with a special low coherence source and a polarization path matching configuration. An expression was derived for the theoretical fringe visibility for on-axis measurement, and the results compared with that of a standard Fizeau interferometer. The visibility for the low coherence Fizeau was found to be near the theoretical maximum for low reference surface reflectivities. Visibility is maximized regardless of test and reference surface reflectivities when input beam balance ratio is equal to 1. Similar to a standard Fizeau, visibility is reduced for higher test surface reflectivities due to multiple cavity reflections. Measurements were made on both sides of an uncoated glass disk without any special treatment or movement and with only two measurements were required. In addition, the thickness of the glass was measured. Using a 15 mW source, the maximum camera exposure time was 150 usec, resulting in very robust vibration insensitivity. The novel arrangement also permits the use of transmission spheres without the need for calibration.

References

1. D. Malacara, M. Servin, and Z. Malacara, "Interferogram analysis for optical testing," (Marcel Dekker, New York, 1998).
2. D. Malacara, *Optical Shop Testing* (Wiley, New York, 1992).
3. P. de Groot, Measurement of Transparent Plates with Wavelength-Tuned Phase-Shifting Interferometry, *Applied Optics* 39 (16), 2658-2663, June 2000.
3. R. Jozwicki, M. Kujawinska, and L. Salbut, "New contra old wavefront measurement concepts for interferometric optical testing," *Optical Engineering* 31, 422 , (1992).
4. J. E. Millerd, N. J. Brock, J. B. Hayes, M. B. North-Morris, M. Novak, and J. C. Wyant, "Pixelated phase-mask dynamic interferometer," *Proc. SPIE* 5531, 304-314, (2004).
5. J. E. Millerd in "Fringe 2005," edited by W. Osten, (Springer, New York, 2005), pg 640.
6. M. Küchel, "Interferometer for measuring optical phase difference," U. S. Patent 4,872,755 (1989).
7. E. Novak, C. Ai, and J. C. Wyant, "Errors caused by nearly parallel optical elements in a laser Fizeau interferometer utilizing strictly coherent imaging," *Proc. SPIE* 3134, 456-460 (1997).
8. J. Shiefman, "Using software to model coherent metrology systems," *Proc. SPIE* 5174, 69-82 (2003).